

Neuron, Volume 108

Supplemental Information

Ultrastructural Imaging of Activity- Dependent Synaptic Membrane- Trafficking Events in Cultured Brain Slices

Cordelia Imig, Francisco José López-Murcia, Lydia Maus, Inés Hojas García-Plaza, Lena Sünke Mortensen, Manuela Schwark, Valentin Schwarze, Julie Angibaud, U. Valentin Nägerl, Holger Taschenberger, Nils Brose, and Benjamin H. Cooper

Neuron, Volume 108

Supplemental Information

Ultrastructural Imaging of Activity- Dependent Synaptic Membrane- Trafficking Events in Cultured Brain Slices

Cordelia Imig, Francisco José López-Murcia, Lydia Maus, Inés Hojas García-Plaza, Lena Sünke Mortensen, Manuela Schwark, Valentin Schwarze, Julie Angibaud, U. Valentin Nägerl, Holger Taschenberger, Nils Brose, and Benjamin H. Cooper

Supplementary Figure 1. Comparative ultrastructural analysis of wild-type mossy fiber-CA3 and Schaffer collateral synapses at different external Ca^{2+} concentrations and in the presence of 1 μM TTX and glutamate receptor blockers in cultured hippocampal roller tube slices.

A-H, 3D Ultrastructural analysis of vesicle pools at active zones (AZs) of mossy fiber-CA3 synapses at 2 mM (dark grey) and 4 mM (green) external Ca^{2+} .

I-O, Ultrastructural analysis of vesicle pools at AZs of Schaffer collateral synapses at 2 mM (dark grey) and 4 mM (green) external Ca^{2+} .

A, I, Frequency distribution plotting the distribution of SVs ($\text{Ø}<60$ nm) within 60 nm of the AZ membrane normalized to AZ area.

B, J, Scatterplot indicating the spatial density of docked SVs (0-2 nm bin) normalized to reconstructed AZ area.

C, K, SV number within 0-40 nm of the AZ normalized to AZ area.

D, Spatial density of docked giant vesicles (GVs; $\text{Ø}>60$ nm) normalized to AZ area.

E, GV number within 0-40 nm of the AZ membrane normalized to AZ area.

F, M, Frequency distribution of vesicle diameters for undocked vesicles within 100 nm of the AZ membrane (2 nm bins). Mossy fiber-CA3 2mM Ca^{2+} , 420 vesicles; Mossy fiber-CA3 4mM Ca^{2+} , 273 vesicles; Schaffer collateral-CA1 2mM Ca^{2+} , 428 vesicles; Schaffer collateral-CA1 4mM Ca^{2+} , 338 vesicles.

G, N, Scatterplot indicating the mean diameter of docked vesicles. Mossy fiber-CA3 2mM Ca^{2+} , 112 vesicles; Mossy fiber-CA3 4mM Ca^{2+} , 76 vesicles; Schaffer collateral-CA1 2mM Ca^{2+} , 140 vesicles; Schaffer collateral-CA1 4mM Ca^{2+} , 109 vesicles.

H, O, Scatterplot indicating the spatial distribution of vesicles with respect to vesicle diameter.

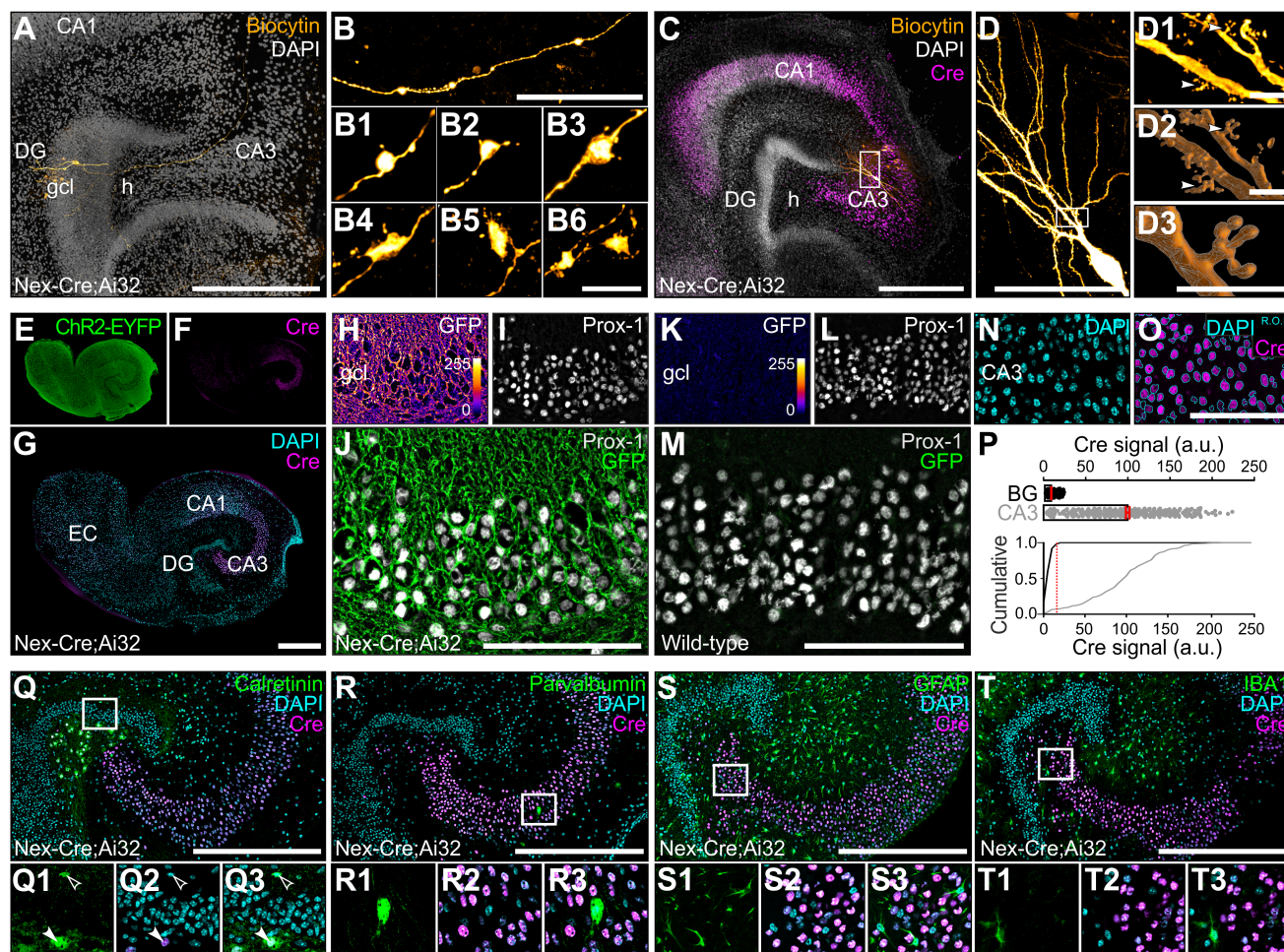
L, Transmission electron micrograph of a Schaffer collateral synapse in the CA1 region of the hippocampus (d, dendrite; m, mitochondrion; psd, postsynaptic density; sp, spine).

P, Q, Electron micrographs acquired in CA3 *stratum lucidum* in which the effect of tissue compression can be appreciated in slices from the same culture prepared by high-pressure freezing using sapphire discs separated by spacer rings of 100 μm (**P**) or 200 μm (**Q**) depth.

Scale bar: **L**, 500 nm; **P** and **Q**, 5 μm . Error bars indicate mean \pm SEM; * $p < 0.05$; ** $p < 0.01$; *** $p < 0.001$; **** $p < 0.0001$. Mossy fiber-CA3 2mM Ca^{2+} , 2 cultures, 2 slices, $n=15$ AZs; Mossy fiber-CA3 4mM Ca^{2+} , 2 cultures, 2 slices, $n=15$ AZs; Schaffer collateral-CA1 2mM Ca^{2+} , 2 cultures, 2 slices, $n=14$ AZs; Schaffer collateral-CA1 4mM Ca^{2+} , 2 cultures, 2 slices, $n=13$ AZs.

See also Table S1A and S1B and Figure 1.

Figure S2



Supplementary Figure 2. Light microscopic analysis of pre- and postsynaptic development of the mossy fiber-CA3 synapse and ChR2 expression in cultured Nex-Cre;Ai32 slices. Related to Figure 1.

A, Maximum projection confocal stack in which post-hoc labelling of an electrophysiologically characterized and biocytin-filled granule cell, reveals the extent of its mossy fiber axonal projection throughout CA3 *stratum lucidum* (orange). Relative positions of dentate gyrus (DG) *stratum granulosum* and CA3 *stratum pyramidale* are shown by nuclear DAPI co-labelling (grey).

B, High magnification confocal z-stacks acquired in *stratum lucidum* reveal large and small *en passant* axonal varicosities (**B**). Large mossy fiber boutons (**B1-B6**) exhibit *in vivo*-like complexity, including fine filopodial extensions.

C, D, Maximum projection confocal stack of a post-hoc immunolabelling of an electrophysiologically characterized and biocytin-filled CA3 pyramidal neuron co-labelled for Cre-recombinase (magenta) and DAPI (grey). In *stratum lucidum*, proximal dendrites of the biocytin-filled cell (**D**, white box enlarged in **D1**) are decorated by complex, multi-compartmental spines (white arrowheads) as visualized in 3D reconstructions (**D2** and **D3**).

E-G, Immunohistochemical labelling against GFP detecting ChR2-EYFP (**E**, green), nuclear Cre-recombinase (**F, G**, magenta) and DAPI (**G**, cyan) in a Nex-Cre;Ai32 cultured slice. Nuclear Cre-recombinase signal is restricted to the *stratum pramidale*.

H-M, Comparative immunohistochemical analysis of membrane-targeted ChR2-EYFP signal (**H, K**, 'fire LUT) distribution within Prox-1 labelled (**I, L**, grey) granule cells of the denate gyrus in Nex-Cre;Ai32 (**H-J**) and wild-type (**K-M**) organotypic slices. In line with earlier findings (Goebbels et al., 2006), granule cells (GCs) of the Nex-Cre knock-in mouse line only transiently express Cre-recombinase and therefore exhibit robust ChR2-EYFP fusion protein expression (**B**), but lack Cre-recombinase immunoreactivity.

N-P, In the CA3 pyramidal cell layer, the vast majority of DAPI stained nuclei (**N**, cyan; **O**, cyan outline) are immunoreactive for Cre-recombinase (**O**, magenta). Scatterplot (**P**, upper) and cumulative distribution (**P**, lower) representing the quantification of nuclear Cre-recombinase signal intensity in non-principal cells (BG, 'background signal') and CA3 pyramidal cells (CA3; 'real signal') in Nex-Cre;Ai32 slice cultures.

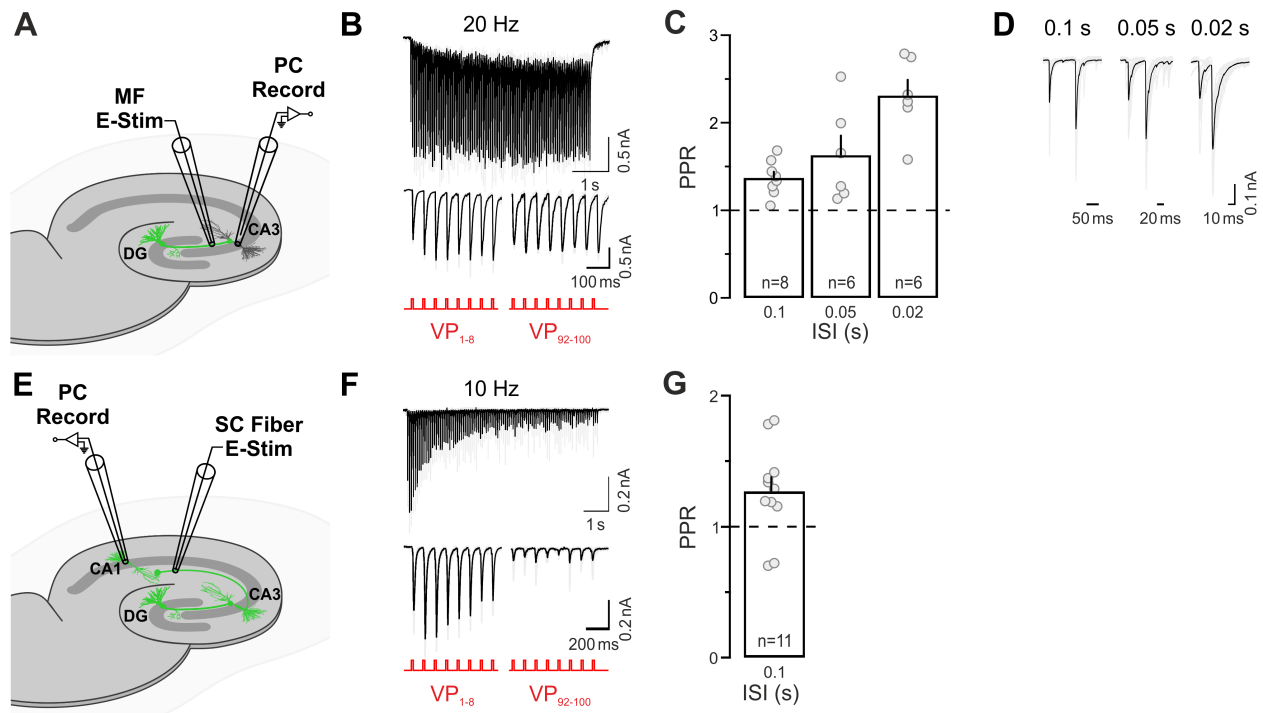
Approximately 93.7% of all CA3 pyramidal cell nuclei have above-threshold (red dashed line) Cre-recombinase expression (**P**, BG, n = 5 slices; 9.3 a.u. \pm 1.29; CA3, n = 5; 99.3 a.u. \pm 2.34). **Q-**

T, Cre-recombinase labelling (magenta) colocalizes with DAPI-positive nuclei (cyan) in calretinin-positive hilar mossy cells (**Q, Q1-Q3**, green, white arrowhead), but is not detectable in

calretinin-positive interneurons (**Q, Q1-Q3**, green, open arrowhead) in the molecular layer of the dentate gyrus, parvalbumin-positive interneurons (**R, R1-R3**, green), GFAP-positive astrocytes (**S, S1-S3**, green), or in IBA1-positive microglia (**T, T1-T3**, green).

Abbrev.: EC, entorhinal cortex; DG, dentate gyrus; CA3, *Cornu Ammonis* Area 3; CA1, *Cornu Ammonis* Area 1; gcl, granule cell layer). Scale bars: **A, C, G, Q-T**, 500 μm ; **B, D, J, M, O**, 100 μm ; **B6**, 10 μm ; **D1**, 5 μm ; **D2, D3**, 2 μm . Error bars indicate mean \pm SEM.

Figure S3



Supplementary Figure 3. Electrophysiological characterization of postsynaptic responses elicited by fiber stimulation of mossy fiber and Schaffer collateral axonal pathways in Dock10-Cre;Ai32 and Nex-Cre;Ai32 organotypic slices, respectively, via glass electrodes filled with external solution. Related to Figure 2.

A, Schematic of the experimental set-up for recording postsynaptic CA3 pyramidal cell (PC) responses to electrical fiber stimulation of the mossy fiber pathway (**B-D**).

B, Excitatory postsynaptic currents (EPSCs) recorded in response to 100 voltage pulses (VPs; 100 μ s duration, 4 to 7 V; 20Hz) in 2 mM Ca^{2+} . Responses to the initial (lower left) and final (lower right) eight stimuli in the train are shown in the bottom panels with an expanded timescale.

C, Paired-pulse ratios measured for different inter-stimulus intervals (ISI) of 0.1 (1.37 ± 0.07 , n= 8), 0.05 (1.63 ± 0.22 , n= 6), and 0.02 (2.31 ± 0.18 , n= 6) seconds.

D, Example traces of EPSCs recorded in response to paired pulses delivered with different inter-stimulus interval (ISI) of 0.1 or 0.05 and 0.02 seconds

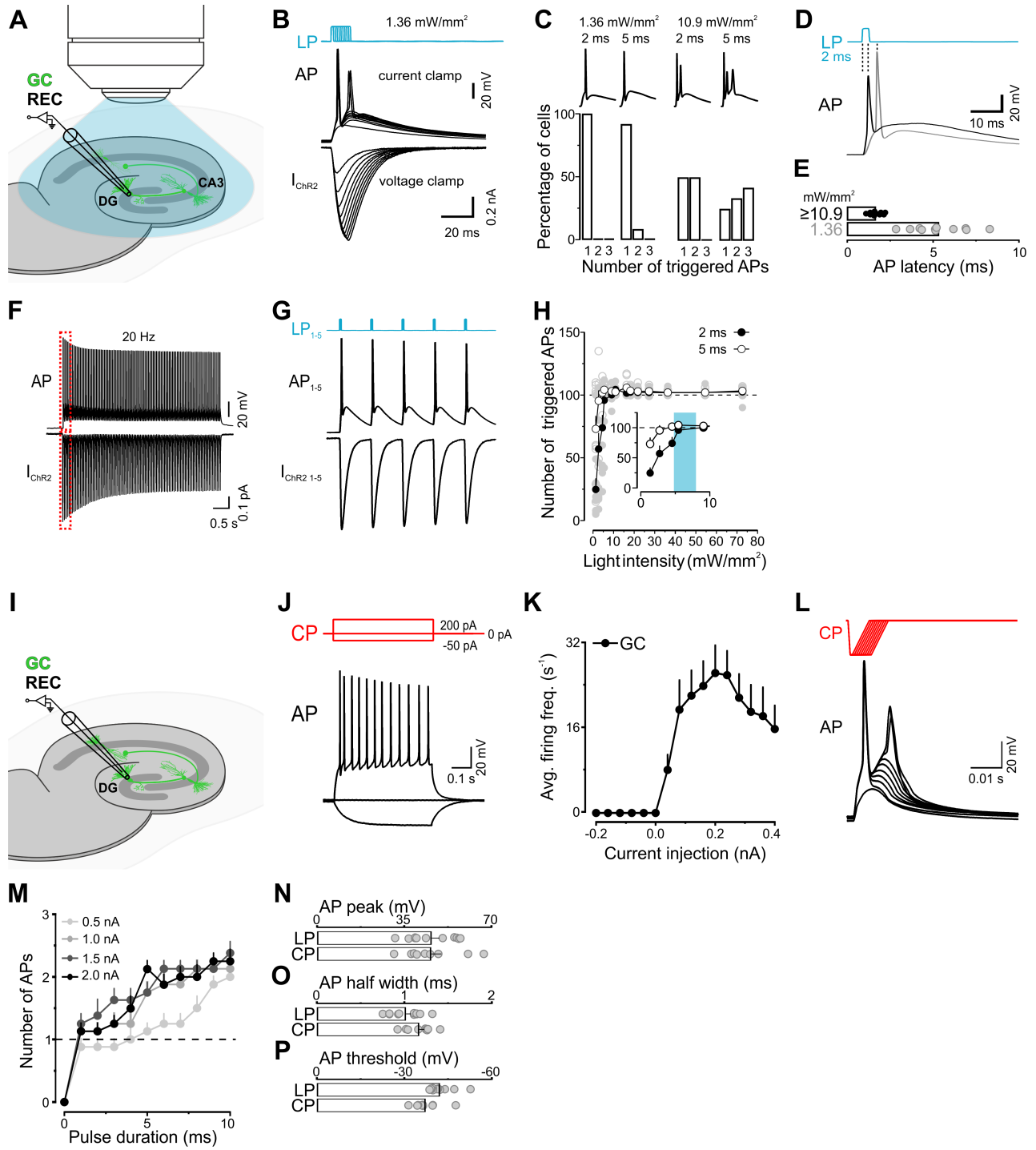
E, Schematic of the experimental set-up for recording postsynaptic CA1 pyramidal cell (PC) responses to electrical fiber stimulation of the Schaffer collateral pathway (**F-G**).

F, EPSCs recorded in response to 100 VPs (10Hz) in 2 mM Ca^{2+} . Responses to the initial (lower left) and final (lower right) eight stimuli in the train are shown in the bottom panels at an expanded timescale.

G, Paired-pulse ratios measured for an interstimulus interval (ISI) of 0.1 second (PPR 1.27 ± 0.10 , n= 11).

Error bars indicate mean \pm SEM.

Figure S4



Supplementary Figure 4. Comparative electrophysiological analysis of the properties of optically and electrically elicited action potentials in dentate gyrus granule cells in Nex-Cre;Ai32 organotypic slices. Related to Figure 2.

A, Schematic illustrating experimental configuration for analyzing AP firing properties of dentate gyrus (DG) granule cells in cultured Nex-Cre;Ai32 slices in response to light stimuli (**B-H**).

B, Exemplary recording of action potentials (APs) in ChR2-expressing hippocampal DG granule cells (GCs) in response to blue light (470 nm) pulses (LPs). For a given light intensity, increasing LP duration (1-10 ms) triggered zero to two APs (upper panel) and a ChR2-mediated current (I_{ChR2}) of increasing size and duration (bottom panel) in this GC.

C, Summary data on AP firing in response to LPs of either 2 ms or 5 ms duration for two light intensities (1.36 mW/mm² and 10.9 mW/mm² (n= 12 cells).

D, E, AP waveform (**D**) and latency (**E**) measured in response to a single 2 ms LP at two light intensities (1.36 mW/mm², 5.35 ± 0.49 ms, n= 11 cells; and ≥ 10.9 mW/mm², 1.67 ± 0.08 ms, n= 11 cells). Latencies are measured from the onset of the light stimulus.

F, G, AP discharge pattern recorded in response to 20 Hz LP trains of 5s duration (100 stimuli) (**F**). All GCs that were excitable by light intensities achievable in the high-pressure freezing chamber were also capable of faithfully following 20 Hz stimulation for at least 100 APs for a large range of light intensities. Traces exemplify an AP train recorded in current-clamp mode (upper panel) and I_{ChR2} recorded in voltage-clamp mode (lower panel) obtained in the same cell in response to 100 LPs (20 Hz, 2 ms pulse duration, light intensities of 5.45 mW/mm² and 1.36 mW/mm² for current-clamp and voltage-clamp, respectively). Note the strong inactivation of I_{ChR2} during the 5 s 20 Hz train. The initial five responses during the trains (**G**, indicated by the red dashed boxes in **F**) are shown at an expanded time scale.

H, Total number of APs triggered in GCs by 100 LP trains (20 Hz) for different light intensities and LP durations (2 ms, n= 11 cells or 5 ms, n= 10 cells). For light intensities >5 mW/mm², an equally high reliability of AP firing was observed in response to trains of 100 LPs of either 2 ms or 5 ms duration. For low light intensities (<5 mW/mm²), 5 ms LP trains yielded a larger total count of APs.

I, Schematic illustrating experimental configuration for measuring AP firing properties in response to injection of depolarizing current pulses (CP) into GCs of cultured Nex-Cre;Ai32 slices (**J-P**).

J, Passive membrane properties and AP firing pattern in response to CP injections of ChR2-expressing hippocampal GCs were characterized under current-clamp conditions by applying families of CPs (500 ms duration, -50 pA initial amplitude, incremented in 50 pA steps).

K, GCs exhibited sustained AP-firing when injecting depolarizing CPs and had a maximum firing frequency of $\sim 25 \text{ s}^{-1}$ (n= 10 cells).

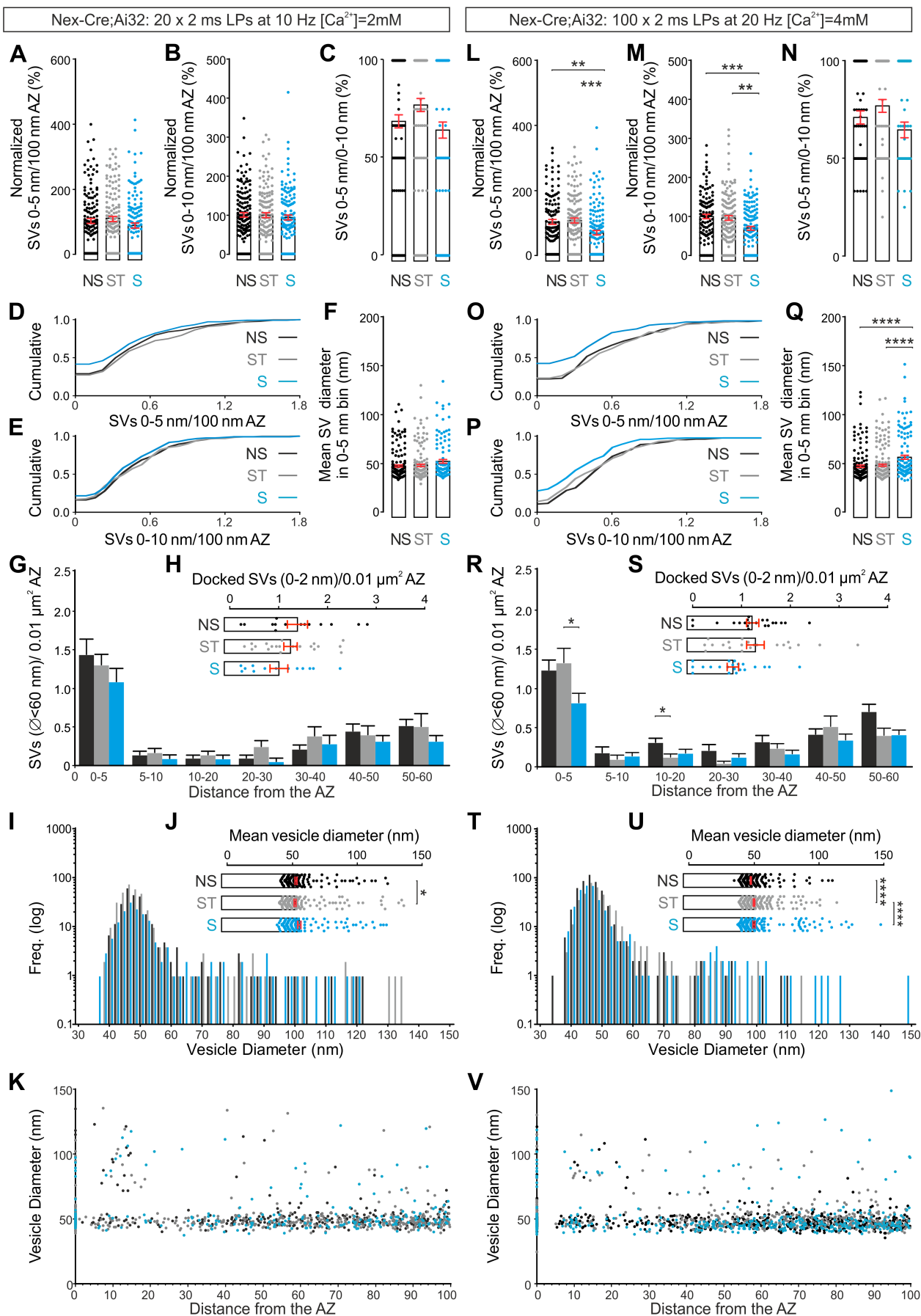
L, AP firing of ChR2-expressing GCs in response to depolarizing CP injections. CPs were composed of two ramps (1 ms rise, 8 ms decay) separated by a plateau of variable duration (1 - 10 ms) to mimic the shape of the ChR2-mediated current (I_{ChR2}) observed under whole-cell voltage-clamp in response to light stimulation (see Figure **S4B**).

M, Depolarizing CP injections of increasing duration and increasing amplitude (0.5 – 2 nA) triggered zero to three APs (n= 8 cells each).

N-P, Comparison of the properties of APs recorded in response to either stimulation by LPs or CP injections. Similar mean values were obtained for both modes of stimulation [**N**, AP peak amplitude: $46.05 \pm 2.84 \text{ mV}$ (LP, n= 11), $45.82 \pm 3.81 \text{ mV}$ (CP, n= 9); **O**, AP half width: $1.02 \pm 0.05 \text{ ms}$ (LP, n= 11), $1.17 \pm 0.05 \text{ ms}$ (CP, n= 9); **P**, AP threshold: $-42.26 \pm 1.26 \text{ mV}$ (LP, n=11), $-37.34 \pm 1.55 \text{ mV}$ (CP, n= 9)].

Error bars indicate mean \pm SEM.

Figure S5



Supplementary Figure 5. Comparative 2D and 3D ultrastructural analyses of mossy fiber-CA3 synapses frozen immediately after mild (20 x 2 ms LPs at 10 Hz; 2 mM Ca²⁺) or strong (100 x 2 ms LPs at 20 Hz; 4 mM Ca²⁺) from cultured Nex-Cre;Ai32 slices.

A-K, 2D (**A-F**) and 3D (**G-K**) ultrastructural analyses of vesicle pools at active zones (AZs) of mossy fiber-CA3 synapses after mild stimulation. NS, no stimulation (black); ST, light stimulation + 1 μ M TTX (grey); and S, light stimulation (blue).

A, B, Spatial density of membrane-proximal vesicles per 100 nm AZ length for vesicles within 0-5 nm (**A**) and 0-10 nm (**B**) of the AZ. Values are normalized to the no stimulation (NS) control condition.

C, Relative proportion of all vesicles within 0-10 nm of the AZ localized within in the 0-5 nm bin.

D, E, Cumulative frequency plots indicating the spatial distribution of membrane-proximal vesicles per 100 nm AZ length for vesicles within 0-5 nm (**D**) and 0-10 nm (**E**) of the membrane.

F, Mean diameter of vesicles within 0-5 nm of the AZ. NS, 181 vesicles; ST, 173 vesicles; S, 118 vesicles.

G, Frequency distributions plotting the distribution of SVs ($\varnothing < 60$ nm) within 60 nm of the AZ membrane normalized to AZ area.

H, Spatial density of docked SVs (0-2 nm bin) normalized to reconstructed AZ area.

I, Frequency distributions of for undocked vesicles within 100 nm of the AZ membrane (2 nm bins). NS, 273 vesicles; ST, 358 vesicles; S, 175 vesicles.

J, Mean diameter of docked (0-2 nm) vesicles. NS, 95 vesicles; ST, 100 vesicles; S, 55 vesicles.

K, Spatial distribution of vesicles with respect to vesicle diameter.

L-V, 2D (**L-Q**) and 3D (**R-V**) ultrastructural analyses of vesicle pools at AZs of mossy fiber-CA3 synapses after strong stimulation.

L, M, Spatial density of membrane-proximal vesicles per 100 nm AZ length for vesicles within 0-5 nm (**L**) and 0-10 nm (**M**) of the AZ. Values are normalized to the no stimulation (NS) control condition.

N, Relative proportion of all vesicles within 0-10 nm of the AZ localized within in the 0-5 nm bin.

O, P, Cumulative frequency plots indicating the spatial distribution of membrane-proximal vesicles per 100 nm AZ length for vesicles within 0-5 nm (**O**) and 0-10 nm (**P**) of the membrane.

Q, Mean diameter of vesicles within 0-5 nm of the AZ. NS, 180 vesicles; ST, 197 vesicles; S, 129 vesicles.

R, Frequency distributions plotting the distribution of SVs ($\varnothing < 60$ nm) within 60 nm of the AZ membrane normalized to AZ area.

S, Spatial density of docked SVs (0-2 nm bin) normalized to reconstructed AZ area.

T, Frequency distributions of for undocked vesicles within 100 nm of the AZ membrane (2 nm bins). NS, 483 vesicles; ST, 375 vesicles; S, 336 vesicles.

U, Mean diameter of docked (0-2 nm) vesicles. NS, 107 vesicles; ST, 134 vesicles; S, 88 vesicles.

V, Spatial distribution of vesicles with respect to vesicle diameter.

2D Analysis (**A-F**): NS, 3 cultures, 4 slices, 44 MFBs, n=144 AZs; ST, 3 cultures, 4 slices, 39 MFBs, n=131 AZs; S, 2 cultures, 3 slices, 36 MFBs, n= 135 AZs.

3D Analysis (**G-K**): NS, 2 cultures, 3 slices, 14 AZs; ST, 2 cultures, 3 slices, n=21 AZs; S, 1 culture, 2 slices, n= 13 AZs.

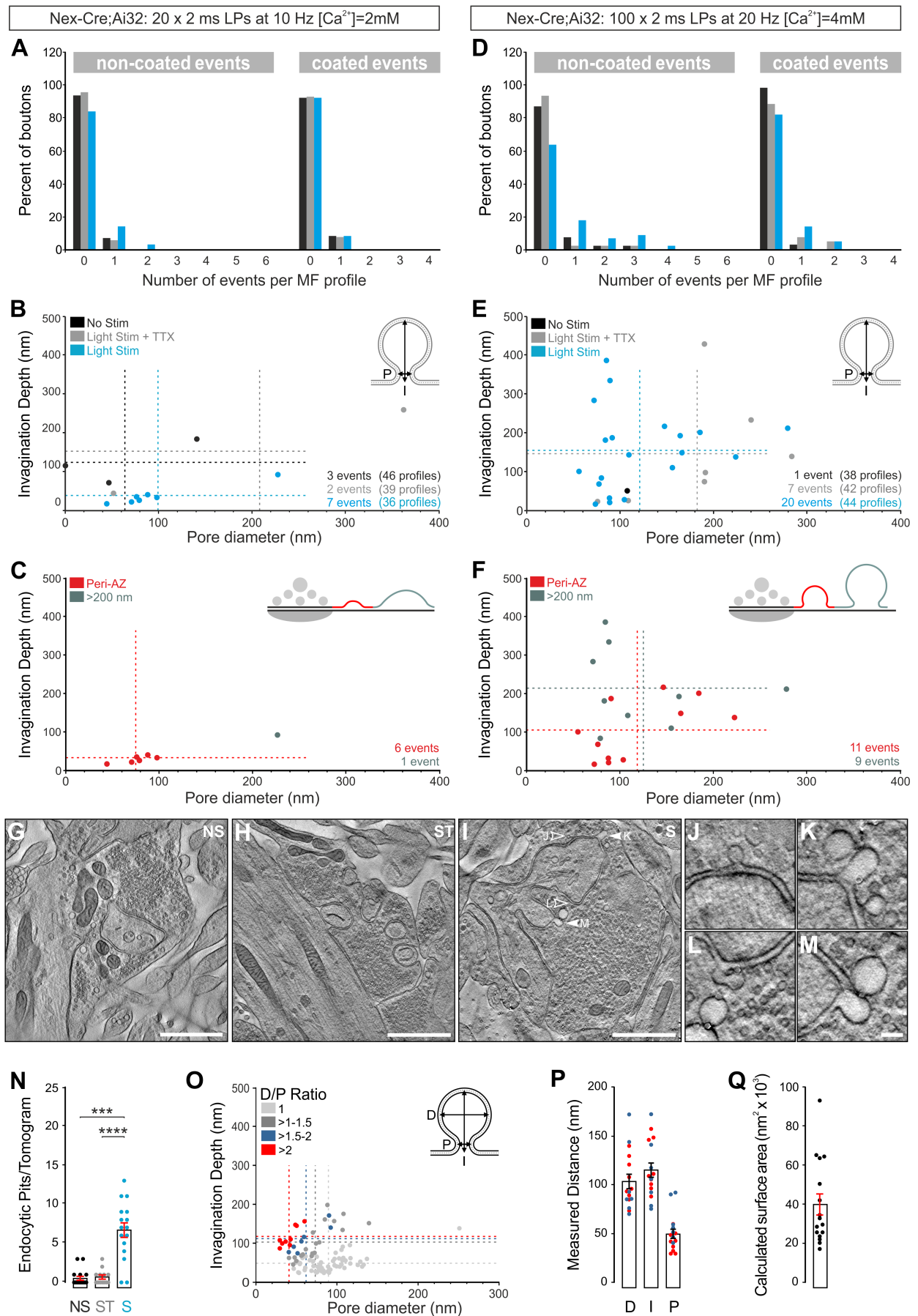
2D Analysis (**L-Q**): NS, 2 cultures, 2 slices, 38 MFBs, n=120 AZs; ST, 2 cultures, 2 slices, 42 MFBs, n=127 AZs; S, 2 cultures, 2 slices, 44 MFBs, n= 139 AZs.

3D Analysis (**R-V**): NS, 2 cultures, 2 slices, n=21 AZs; ST, 2 cultures, 2 slices, n=21 AZs; S, 2 cultures, 2 slices, n= 21 AZs.

Error bars indicate mean \pm SEM; *p < 0.05; **p < 0.01; ***p<0.001; ****p < 0.0001.

See also Figures 4 and 5 and Table S1G-S1J.

Figure S6



Supplementary Figure 6. Comparative 2D and 3D ultrastructural analyses of endocytic profiles in mossy fiber-CA3 synapses frozen immediately after mild (20 x 2 ms LPs at 10 Hz; 2 mM Ca²⁺) or strong (100 x 2 ms LPs at 20 Hz; 4 mM Ca²⁺) from cultured Nex-Cre;Ai32 slices.

A-C, 2D ultrastructural analyses of endocytic profiles in mossy fiber-CA3 synapses after mild stimulation. NS, no stimulation (black); ST, light stimulation + 1 μ M TTX (grey); and S, light stimulation (blue).

D-F, 2D ultrastructural analyses of endocytic profiles in mossy fiber-CA3 synapses after strong stimulation.

A, D, Histogram plotting the relative incidence of coated and non-coated membrane invaginations observed in the three experimental conditions: NS, no stimulation (black); ST, light stimulation in the presence of 1 μ M TTX (grey); and S, light stimulation (blue).

B-F, Relationship between pore diameter (P) and invagination depth (I) for non-coated endocytic intermediates across all conditions (**B, E**) and for non-coated endocytic intermediates detected exclusively in stimulated mossy fiber boutons at peri-active zonal (red) and more distally localized (green) sites (**C, F**). Dashed lines indicate respective mean values.

G-Q, 3D ultrastructural analyses of endocytic profiles in mossy fiber-CA3 synapses after strong stimulation.

G-I, Representative electron tomographic subvolumes acquired at 5000x magnification from 350 nm-thick sections through MFBs from three experimental conditions: NS, no stimulation (**G**), ST, stimulation in the presence of 1 μ M TTX (**H**), and S, stimulation (**I**).

J-M, Manipulation of tomographic slice tilt angles revealed the shape and full extent of individual membrane invaginations indicated in **I**.

N, Relative incidence of putative endocytic profiles per tomogram.

O, Relationship between pore diameter (P) and invagination depth (I) according to the ratio of maximum diameter (D) and pore diameter (D/P= 1, light grey; D/P= >1-1.5, dark grey; D/P= 1.5-2, blue; D/P= >2, red; respective mean values indicated by dashed lines).

P, Scatterplot indicating parameters (D, maximum diameter; I, invagination depth; P, pore diameter) pooled from endocytic events with D/P ratios of 1.5-2 (blue) and >2 (red) for pore diameters < 100 nm.

Q, Calculated surface area of predicted endocytosed vesicles from profiles with D/P ratios >1.5.

Scale bars: **G-I**, 1 μm ; **M**, 100 nm. Error bars indicate mean \pm SEM; *** $p < 0.001$; **** $p < 0.0001$.

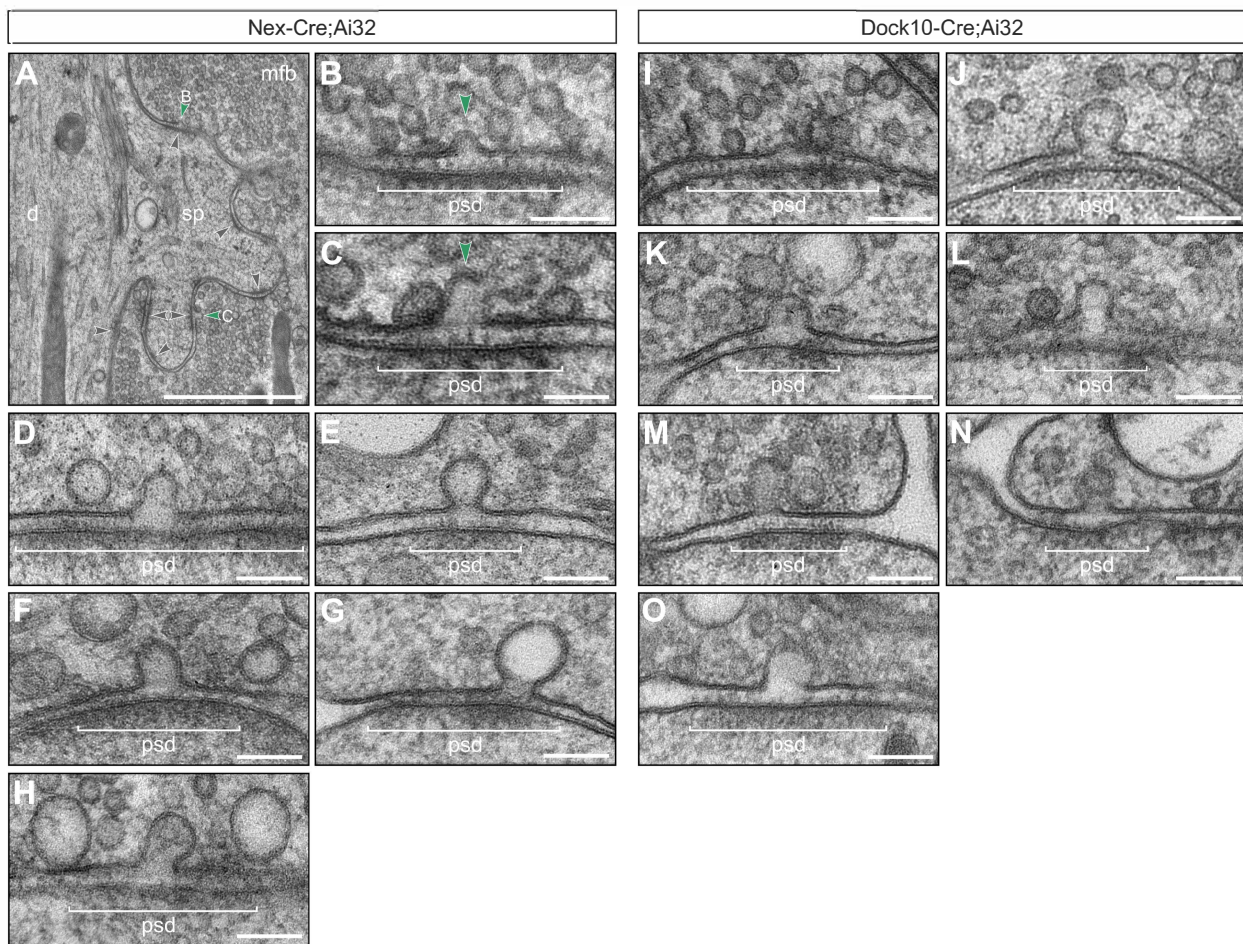
2D Analysis (**A-C**): NS, 3 cultures, 4 slices, 47 MFBs; ST, 3 cultures, 4 slices, 39 MFBs; S, 2 cultures, 3 slices, 36 MFBs.

2D Analysis (**D-F**): NS, 3 cultures, 4 slices, 38 MFBs; ST, 3 cultures, 4 slices, 42 MFBs; S, 2 cultures, 3 slices, 36 MFBs.

3D Analysis (**G-Q**): NS, 2 cultures, 2 slices, $n=17$ tomograms; ST, 2 cultures, 2 slices, $n=13$ tomograms; S, 2 cultures, 2 slices, $n=16$ tomograms.

See also Figures 6 and 7, Table S1K-S1M and Video S2.

Figure S7



Supplementary Figure 7. Omega-profiles detected directly at mossy fiber presynaptic active zones in optically stimulated Nex-Cre;Ai32 and Dock10;Ai32 slices.

A-C, Active zone (AZ) localized omega profiles (green arrowheads) observed in direct apposition to the postsynaptic density (**A**, black arrowheads; **B-C**, psd) in stimulated Nex-Cre;Ai32 slices (20x 2 ms LPs at 10 Hz; 2 mM Ca²⁺).

D-H, AZ localized omega profiles observed in direct apposition to the postsynaptic density (psd) in stimulated Nex-Cre;Ai32 slices (100 x 2 ms LPs at 20 Hz; 4 mM Ca²⁺).

I-O, AZ localized omega profiles observed in direct apposition to the postsynaptic density (psd) in stimulated Dock10-Cre;Ai32 slices (100 x 5 ms LPs at 20 Hz; 2 mM Ca²⁺).

Abbrev.: d, dendrite; mfb, mossy fiber bouton; sp, complex spine; psd, postsynaptic density. Scale bars: **A**, 1 µm; **B-O**, 100 nm.

See also Figure 6.